WATER RESOURCES RESEARCH, VOL. 37, NO. 10, PAGES 2481–2491, OCTOBER 2001

Solute transport along preferential flow paths in unsaturated fractures

Grace W. Su
U.S. Geological Survey, Menlo Park, California, USA

Jil T. Geller and Karsten Pruess
Earth Sciences Division, Lawrence Berkeley National Laboratory, Berkeley, California, USA

James R. Hunt
Department of Civil and Environmental Engineering, University of California, Berkeley, California, USA

Abstract. Laboratory experiments were conducted to study solute transport along preferential flow paths in unsaturated, inclined fractures. Qualitative aspects of solute transport were identified in a miscible dye tracer experiment conducted in a transparent replica of a natural granite fracture. Additional experiments were conducted to measure the breakthrough curves of a conservative tracer introduced into an established preferential flow path in two different fracture replicas and a rock-replica combination. The influence of gravity was investigated by varying fracture inclination. The relationship between the travel times of the solute and the relative influence of gravity was substantially affected by two modes of intermittent flow that occurred: the snapping rivulet and the pulsating blob modes. The measured travel times of the solute were evaluated with three transfer function models: the axial dispersion, the reactors-in-series, and the lognormal models. The three models described the solute travel times nearly equally well. A mechanistic model was also formulated to describe transport when the pulsating blob mode occurred which assumed blobs of water containing solute mixed with residual pools of water along the flow path.

1. Introduction

Rock fractures in the unsaturated zone can provide fast pathways for the transport of contaminants into the groundwater. Laboratory, field, and theoretical studies have demonstrated that flow proceeds along localized preferential flow paths, or fingers, through unsaturated fractures [e.g., *Glass*, 1993; *Nicholl et al.*, 1994; *Pruess*, 1998; *Su et al.*, 1999; *Dahan et al.*, 1999]. Preferential flow paths can dramatically decrease the residence times of contaminants compared to conceptual models that predict spatially uniform flow in fractures, subject to strong capillary imbibition effects from the rock matrix that draws the flowing liquid from the fracture [*Nitao and Buscheck*, 1991; *Wang and Narasimhan*, 1985]. Transport of dissolved radionuclides along preferential flow paths in unsaturated fractures is a concern at Yucca Mountain, Nevada, a site currently being evaluated as a potential nuclear waste repository. Evidence of fast flow through the unsaturated zone at Yucca Mountain was observed by *Fabryka-Martin et al.* [1996], where elevated levels of bomb pulse ^{36}Cl were measured at ~300-m depth, indicating that infiltrating water had reached those depths within only 50 years.

Mechanisms controlling liquid flow in unsaturated fractures have been examined in a number of laboratory experiments [e.g., *Nicholl et al.*, 1994; *Tokunaga and Wan*, 1997; *Su et al.*, 1999; *Geller et al.*, 2000]. Glass and coworkers have conducted an extensive analysis of fingered flow in unsaturated fractures [see *Glass and Nicholl*, 1996, and references therein]. Laboratory studies of solute transport in unsaturated fractures have been very limited, however. A number of field transport experiments have been performed in unsaturated fractured rocks [e.g., *Liu et al.*, 1995; *Nativ et al.*, 1995; *Dunnivant et al.*, 1998], but interpretation of field measurements is often problematic because detailed characterization of the subsurface is difficult. Data from laboratory experiments are generally easier to interpret than data from the field since conditions are controlled and the system is easier to characterize. In addition, laboratory experiments complement field and numerical studies by furthering the understanding of smaller-scale mechanisms which may affect processes at a larger scale. Models of solute transport that employ continuum concepts and the advection-diffusion equation [e.g., *Doughty*, 1999] may not be applicable for describing some important flow processes affecting transport in unsaturated fractured media, such as fingered flow. *Glass et al.* [1989] found that solute transport was difficult to describe using the advection-dispersion equation when flow occurred along fingers in homogeneous sand. Temporal flow instabilities in unsaturated, inclined fractures have been observed in laboratory experiments [*Glass and Nicholl*, 1996; *Su et al.*, 1999] and are not predicted by current flow and transport models.

The objective of this paper is to examine the effect of gravity and small-scale flow instabilities on solute transport along preferential flow paths in unsaturated, variable-aperture fractures. A miscible dye tracer experiment is conducted in a transparent

Paper number 2000WR000093.
0043-1397/01/2000WR000093$09.00

epoxy replica of a natural granite fracture to identify the qualitative features of transport. Breakthrough curves of a conservative tracer demonstrate different flow regimes depending upon the relative influence of gravity along an established flow path. These breakthrough curves are analyzed with three transfer function models, and a mechanistic model is also developed to describe solute transport when flow undergoes cycles of snapping and reforming, or intermittent flow.

2. Solute Transfer Functions

Because of the complexity of flow in unsaturated fractures, transfer functions have been suggested as a potential alternative to describe transport through fractured rock at the field scale [*Chesnut*, 1992; *Pruess et al.*, 1999]. This approach simplifies complex systems by characterizing the output solute flux as a function of the input flux [*Jury*, 1982; *Jury and Roth*, 1990]. The simplicity of the transfer function makes it an appealing alternative to continuum-based models of unsaturated flow. The transfer function has been successful in describing solute transport in unsaturated, heterogeneous soils at the laboratory and field scale [e.g., *Jury et al.*, 1990; *Zhang*, 1995] even though assumptions about flow mechanisms are not accounted for using this approach.

For solute transport the transfer function is the probability density function (pdf) of the solute travel times. In chemical reactor modeling the pdf is referred to as the residence time distribution instead of the transfer function [*Levenspiel*, 1972]. The transfer functions that will be used to analyze the solute breakthrough curves in this study are the axial dispersion, the reactors-in-series, and the lognormal models. The pdf's of the solute travel times can be characterized by the first and second moments of the pdf's, which are defined respectively, as

$$\mu = \int_0^\infty tE(t)\,dt \tag{1}$$

$$\sigma^2 = \int_0^\infty (t-\mu)^2 E(t)\,dt, \tag{2}$$

where $E(t)$ is the pdf of the system for a pulse input (delta function), t is time, μ is the first moment of the pdf, and σ^2 is the second moment.

2.1. Axial Dispersion Model

The axial dispersion transfer function model is derived from the one-dimensional advection-dispersion equation. It is assumed that the medium is homogeneous and that the velocity and dispersion coefficient are constants in the domain studied. The pdf of this model is given by [*Levenspiel*, 1972]

$$E(t) = \frac{1}{2\sqrt{\pi}}\left(\frac{Pe}{t_m t}\right)^{1/2} \exp\left[-\frac{t_m Pe}{4t}(1-t_m)^2\right], \tag{3}$$

where t_m is the mean residence time given theoretically by L/v, where L is the longitudinal length of the system and v is the pore fluid velocity. Pe is the Peclet number and is defined as

$$Pe = \frac{vL}{D}, \tag{4}$$

where D is the dispersion coefficient. The first moment of the axial dispersion model with open boundaries is given by

$$\mu = t_m\left(1 + \frac{2}{Pe}\right). \tag{5}$$

The second moment for this model is given by

$$\sigma^2 = t_m^2\left(\frac{2}{Pe} + \frac{8}{Pe^2}\right). \tag{6}$$

Information on the first and second moments allows one to determine the two unknown parameters in the axial dispersion model, t_m and Pe.

2.2. Reactors-in-Series Model

In the reactors-in-series model the system is modeled as a series of perfectly mixed volumes of equal size. The pdf for n reactors in series is given by [*Levenspiel*, 1972]

$$E_n(t) = \frac{1}{(n-1)!}\frac{t^{n-1}}{\left(\frac{\mu}{n}\right)^n}\exp\left(-\frac{nt}{\mu}\right). \tag{7}$$

The first moment of this model is equal to the mean residence time of the solute, and the second moment is a function of n and μ:

$$\sigma^2 = \frac{\mu^2}{n}. \tag{8}$$

When measurements provide data to determine μ and σ^2, then (8) provides the best estimate of the number of reactors, n.

2.3. Lognormal Transfer Function

The lognormal transfer function has been successful in predicting pdf's in unsaturated, heterogeneous porous media [*Jury*, 1982] and has also been suggested to model pdf's in heterogeneous fractured media [*Chesnut*, 1992]. The pdf for the lognormal transfer function is [*Jury*, 1982]

$$E(t) = \frac{1}{t\sqrt{2\pi}\sigma_{\ln t}}\exp\left\{-\frac{1}{2}\left[\frac{1}{\sigma_{\ln t}}\ln\left(\frac{t}{\mu_{\ln t}}\right)\right]^2\right\}. \tag{9}$$

The first and second moments of a lognormally distributed function are defined as [*Benjamin and Cornell*, 1970]

$$\mu = \mu_{\ln t}\exp\left(\frac{1}{2}\sigma_{\ln t}^2\right) \tag{10}$$

$$\sigma^2 = \mu^2[\exp(\sigma_{\ln t}^2) - 1], \tag{11}$$

where $\mu_{\ln t}$ is the first moment of logarithmic t and $\sigma_{\ln t}^2$ is the second moment of logarithmic t.

3. Apparatus and Experimental Procedures

Four tracer experiments were performed in this study with the conditions summarized in Table 1. A miscible dye tracer experiment was performed in experiment 1 to qualitatively examine transport along a preferential flow channel. The established flow channel was initially saturated with dyed water (0.2% Liquitint by volume, Milliken Chemical, Inman, South Carolina) before clear water was introduced into the flow channel at the same flow rate. Chemical properties of the dyed water are summarized by *Su et al.* [1999]. Experiments 2–4 were conducted to determine pdf's of a conservative tracer

Table 1. Summary of Experimental Conditions

Experiment	Description	Flow Cell[a]	Q, mL h^{-1}	β, deg
1	miscible dye tracer test	epoxy replica I	5	47
2	solute transport and breakthrough curves	epoxy replica II	3, 5	20, 45, 80
3	solute transport and breakthrough curves	epoxy replica I	5	20, 80
4	solute transport and breakthrough curves	rock-epoxy replica	5	20, 45, 80

[a]Epoxy replicas I and II were made from the same fracture.

along an established preferential flow path in an unsaturated fracture.

An epoxy replica of a natural granite fracture from the Stripa Mine in Sweden was used in experiments 1–3. The procedures for fabricating these epoxy replicas are detailed by *Persoff and Pruess* [1995]. The same replica was used in experiments 1 and 3 and is denoted as epoxy replica I in Table 1. A different replica of the same rock fracture, epoxy replica II, was used in experiment 2. In experiment 4, one half of an actual granite rock fracture, also from the Stripa Mine in Sweden, was mated to an epoxy replica of the other half (rock-replica). The fracture used in the rock-replica experiments was a different sample than the one used in experiments 1–3. The rock-replica combination was used to incorporate the effect of the surface chemistry of the rock while still providing for flow imaging. Contact angle measurements of water on epoxy and smoothed granite using the capillary rise method resulted in values of ~63° for the epoxy and ~60° for the granite [*Geller et al.*, 1996]. Spreading of a water drop was observed on a fracture surface of the same rock used in the contact angle measurements, indicating that small-scale roughness and near-surface porosity along the surfaces of natural rock fractures may play an important role on wetting behavior [*Geller et al.*, 1996].

Before each experiment the flow cells were washed with distilled, deionized water. The epoxy replica surfaces were then rinsed with methanol and allowed to air dry, while the rock fracture surface was allowed to air dry for ~20 hours after it had been washed with water. The relative humidity of the room was around 50% and the temperature was ~20°C. The dimensions of the replica-only fracture were 21.5 × 33 cm, while the rock-replica fracture had dimensions of 18.5 × 20.5 cm. The fracture replica and rock-replica were loaded between an aluminum frame with six confining bolts and then mounted over an inclined light table. Fracture aperture statistics were not measured in these experiments, but prior analysis performed for this type of fracture resulted in a mean aperture of 0.16 ± 0.11 mm [*Su et al.*, 1999]. Observations from the experiments were obtained with a video camera (JVC KY-F55BU with lens JVC TY-10×6 MDPU). The video recorder (Sony SVHS SVO-5800) had time coding, which provided a temporal resolution of 1/30 s. Water was supplied at a constant flow rate, Q, with a syringe pump (Model 33, Harvard Apparatus, South Natick, Maine). A schematic of the experimental apparatus is shown in Figure 1.

The angle of inclination, β, was changed without reassembling the fracture in experiments 2–4. At each angle a flow path in the fracture was allowed to establish to a given flow rate for ~24 hours before a step input of a 0.5 g L^{-1} chloride tracer solution was introduced. The syringe pump operated two syringes, one containing distilled, deionized water and the other containing the tracer solution. The water and the tracer solution were not dyed during these experiments. A three-way valve near the inlet of the fracture was used to switch from distilled water to the tracer solution without interrupting the flow. Breakthrough curves of the tracer were obtained by measuring the conductance of the water at the outlet of the fracture using gold wire electrodes. The conductance at the inlet of the fracture was also measured to determine the time when the tracer reached the fracture inlet. Each electrode consisted of two 10-mm lengths of 0.2-mm diameter gold wire separated by 10 mm. The wires were glued to plastic endcaps and connected to a data acquisition board (Model UPC601-U, Validyne Engineering Corp., Northridge, California) which recorded the data to a computer. The endcaps contained fittings for injecting and collecting water. Detail of the endcap is also shown in Figure 1. Filter paper (Whatman glass microfibre filters GF/D, Clifton, New Jersey) was placed along the inlet and outlet of the fracture, and the endcaps were placed directly over the filter paper. A small piece of filter paper was placed along the center of the fracture inlet to provide capillary continuity as water was introduced into the fracture. Three pieces of filter paper were placed at the outlet to prevent water buildup. The volume of water contained in each saturated piece of filter paper at the inlet and outlet was around 0.15 cm^3. The volume of water in the inlet tubing displaced by the tracer solution was ~0.1 cm^3. The amount of solute mixing that occurred in the inlet was small since the measured input signal was approximately a step function.

Comparison of the density-driven and gravity-driven velocities indicates whether buoyancy effects are likely to be significant upon switching to the tracer solution during experiments 2–4. The ratio of the gravity-driven velocity (u_{grav}) to the density-driven velocity ($u_{density}$) must be much greater than 1 for buoyancy effects to be negligible:

$$\frac{u_{grav}}{u_{density}} = \frac{\rho_w}{\rho_s - \rho_w} \gg 1, \tag{12}$$

where ρ_w is the density of water and ρ_s is the density of the solute solution. The density of water at 20°C is 998.2 kg m^{-3}. The density of a solution with a sodium chloride concentration of 0.5 g L^{-1} is 1.0041 times greater than the density of water [*Chemical Rubber Company*, 1994]. Using these values, the magnitude of the ratio in (12) is 244, indicating that buoyancy effects are not significant.

4. Results

This section summarizes the results from the miscible tracer test and the solute transport experiments. Analyses of the

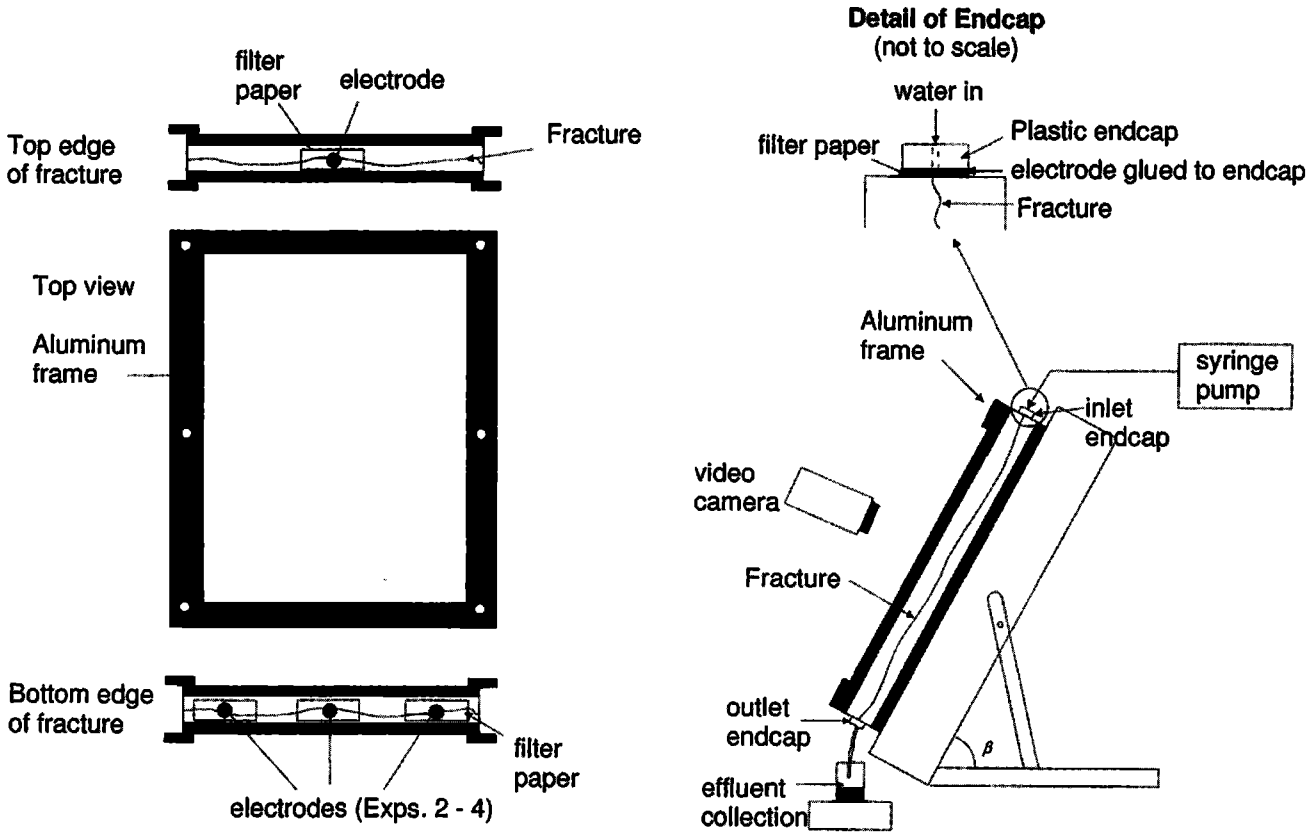

Figure 1. Schematic of experimental setup.

breakthrough curves (BTCs) from the solute transport experiments are also presented.

4.1. Miscible Dye Tracer Test

Images from the miscible dye tracer test (experiment 1) are shown in Figure 2, where the clear water is introduced into the preferential flow path containing dyed water. The flow channels are clearly shown in Figure 2a when steady flow of dyed water was established. Wider regions of liquid, or capillary pools, are connected to narrow channels, or rivulets of liquid. Similar features of steady flow were also observed in other flow visualization experiments conducted in an unsaturated fracture replica [*Su et al.*, 1999]. The dyed solution is displaced from the main flow paths in the upper half of the fracture after 67.2 s of clear water flow (Figure 2b). Dye is mostly displaced from the lower flow channels after 154.8 s (Figure 2c). The dye is completely displaced from the flow channels after 450 s of steady flow but remains behind in isolated pools not connected to the flow path. The persistence of dyed water over time along the edges of the flow path shows that faster flowing regions occur along the center. Diffusion and dispersion of the dye occur in the flow path as evidenced by the gradual change in the dye concentration over time. Capillary pools act as long-term sources and/or sinks for the tracer, while rivulets transport the tracer more rapidly since they are so narrow.

4.2. Solute Transport Experiments

Flow was intermittent within the fractures in experiments 2 and 3 even though the influent flow rate was constant. Figure 3 shows four sketches of the liquid distribution during one cycle of intermittent flow during experiment 2. Figure 3a was recorded 2 s after the rivulet snapped. The end of the upper rivulet has begun to fill with liquid after 12 s, forming a blob of liquid, while the lower rivulet has drained into the lower pool (Figure 3b). The blob of liquid begins to move downward at 18 s (Figure 3c), and the flow channel (rivulet) is connected at 21 s (Figure 3d). This type of intermittency will be referred to as the snapping rivulet mode, where flow is steady for some time over the length of the fracture before rivulets suddenly snap and reform. Intermittent flow was also observed in experiment 3. The sequence of fluid outlines shown in Figure 4 indicates blob growth (Figure 4a), blob before detachment (Figure 4b), detached blob coalescing with pool (Figure 4c), pool drainage out of the bottom (Figure 4d), and growth of a new blob at the top (Figure 4e). This type of intermittency will be referred to as the pulsating blob mode because flow occurs as a series of blobs and the flow channel never becomes completely connected over the length of the fracture. The snapping rivulet mode and pulsating blob mode were also observed in experiments summarized by *Su et al.* [1999]. In experiment 4, direct observations of the flow distribution indicated that the flow channel was steady at inclinations of 20° and 45° and was intermittent at 80°. Although experiments 1 and 3 were conducted on the same fracture replica and had similar conditions, reassembling the fracture replica between experiments can cause subtle changes in the aperture distribution. The location of the flow channel and the occurrence of intermittent flow in these experiments were subsequently affected by this.

Solute transport was quantified in experiments 2–4 by measuring the BTCs of a conservative tracer. The BTCs from experiments 2–4 are presented in Figure 5. The electrical con-

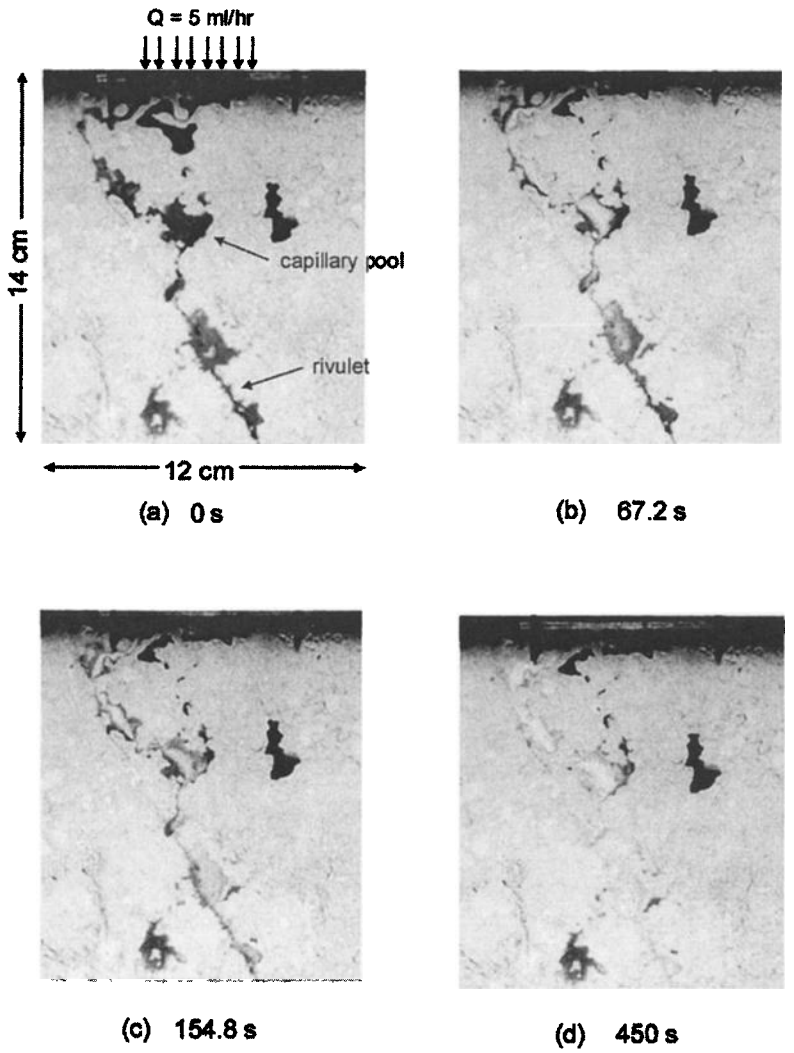

Figure 2. Images from experiment 1 (a) before clear water was introduced and (b)–(d) at various times after clear water was introduced. Faster-flowing regions through the center of the flow path are evidenced by the persistence of dye along the edges of the flow channel. Dyed water along the flow path has been nearly flushed out by the clear water in Figure 2d.

ductance of the effluent solute was normalized by the maximum electrical conductance measured to obtain the relative solute concentration. Calibration verified that the electrical conductance was linearly related to the solute concentration.

The BTCs from experiments 2 and 4 have an S-shaped curve as expected for a step input function of solute at all the angles of inclinations and flow rates. Tailing is also evident in these BTCs by the gradual rise to maximum concentration and is due

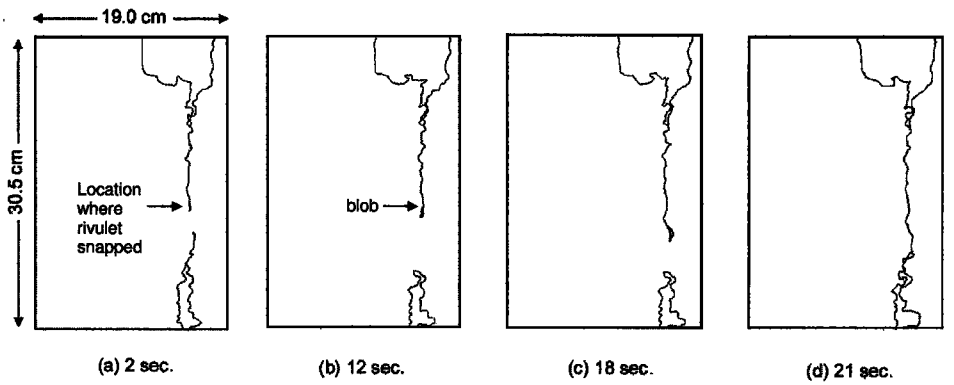

Figure 3. Liquid distribution during experiment 2, $\beta = 45°$, $Q = 5$ mL h^{-1}. One cycle of intermittent flow is shown in the sequence of images. Time denotes seconds after the rivulet had snapped.

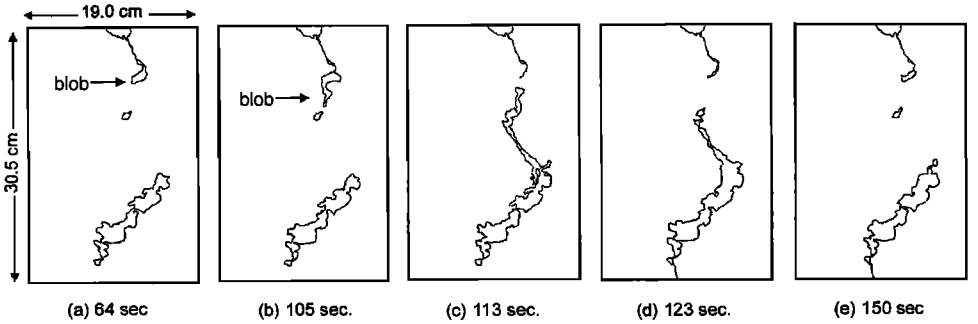

Figure 4. Liquid distribution during experiment 3, $\beta = 80°$, $Q = 5$ mL h^{-1}. One cycle of intermittent flow is shown in the sequences of images. Time denotes seconds after the previous blob had disconnected from the flow channel.

to solute mixing in the capillary pools, as observed in the miscible dye tracer experiment. The BTCs from experiment 3 have very large fluctuations due to intermittent flow occurring in this experiment with a low frequency. The peaks in the BTCs occur whenever a blob of water from an intermittent event reaches the filter paper at the outlet. The fluctuations in the BTCs from experiments 2 and 4 were not as pronounced, even though intermittent flow occurred in these experiments, because the frequency of water in contact with the outlet was relatively high compared to experiment 3.

The BTCs from experiment 2 at 3 mL h^{-1} do not overlap at the different angles of inclination (Figure 5a), while the BTCs at 5 mL h^{-1} are almost identical at all three angles of inclination (Figure 5b), except during the early breakthrough times, where there are slight differences at each angle. The trend of the travel times of the solute as a function of angle of inclination is unexpected. At both flow rates the lowest angle has the fastest initial breakthrough, while the highest angle has the slowest initial breakthrough, which is contrary to what we would expect as the relative influence of gravity increases. The reason for the unexpected trend in the travel times as a function of gravity is the occurrence of the snapping rivulet mode. In this mode the total time that the flow channel was disconnected increased at the higher angles, slowing the solute travel to the outlet and thereby increasing the travel time.

The fluctuations in the recorded solute concentrations for these experiments reflect a change in solute concentration as well as a change in water content of the filter paper. The electrodes are in contact with the filter paper at the outlet, and the conductance of the filter paper changes because of changes in salt concentration and because the water saturation in the filter paper decreases between intermittent events. The changes in solute concentrations in experiment 3 (Figure 5c) are particularly pronounced because the frequency of water in contact with the outlet was considerably lower compared to the other experiments. Because of these large fluctuations the average concentration of each pulse obtained from Figure 5c is plotted as a function of time in Figure 5d. The initial pulse arrival of solute has values of 20 and 40% of the maximum inlet solute concentration before increasing gradually. In this experiment the travel times decrease with increasing angle of inclination, consistent with expectations. Since the pulsating blob mode occurred, the travel time of the solute was controlled by how quickly the disconnected blob reached the outlet. The velocity of the blobs increases as the relative influence of gravity increases.

In experiment 4 the solute travel times decrease as the inclination increases from 20° to 45° under steady flow conditions. At an inclination of 80° the flow is intermittent, and a longer travel time is observed. The increase in solute travel times at 80° is attributed to flow changing from a steady flow regime at the two lower angles to an intermittent flow regime at 80°. Experiment 4 shows that intermittent flow may increase travel times compared to steady flow.

In order to summarize the results of experiments 2–4 the average travel times were obtained from each of the BTCs and are presented in Table 2. The average travel time (t_{ave}) is defined as the time it takes for the solute to reach one half of its final concentration. The two epoxy fractures have a different length than the rock-replica fracture; therefore, in order to compare the results from all experiments the average velocities (u_{ave}) of the solute were calculated by dividing the total length of the fracture by the average travel time. At a flow rate of 5 mL h^{-1}, similar average velocities were measured in the three different fractures at 20°. At 80° the average velocity varied by as much as a factor of 2 in the different experiments.

4.3. Analysis of Breakthrough Curves: Experiments 2 and 4

The three transfer function models used to evaluate the measured BTCs are written for a delta function input (equations (3), (7), and (9)). Since the measured data comes from a step function input, differentiation of the BTCs to obtain the pdf's of the travel times was performed to analyze the results:

$$E(t) = \frac{C(t + dt) - C(t)}{C_0 dt}, \tag{13}$$

where the numerator in (13) is the difference in the concentration between two successive time periods, C_0 is the inlet solute concentration, and dt is the time interval between these measurements. Before the measured BTCs were differentiated, fluctuations in the BTCs were smoothed by averaging the data over 2-min intervals in experiment 2 and a 1-min interval in experiment 4. The results from experiment 3 will be analyzed in the next section because of the large period fluctuations. The pdf's obtained from experiments 2 and 4 are shown in Figures 6a–6c for $\beta = 45°$. The pdf's are not symmetrical and have peaks at the early times. The first and second moments are summarized in Table 3. The calculated parameters used in the axial dispersion, the reactors-in-series, and the lognormal models are also presented in Table 3. The curves corresponding to the different transfer function models are

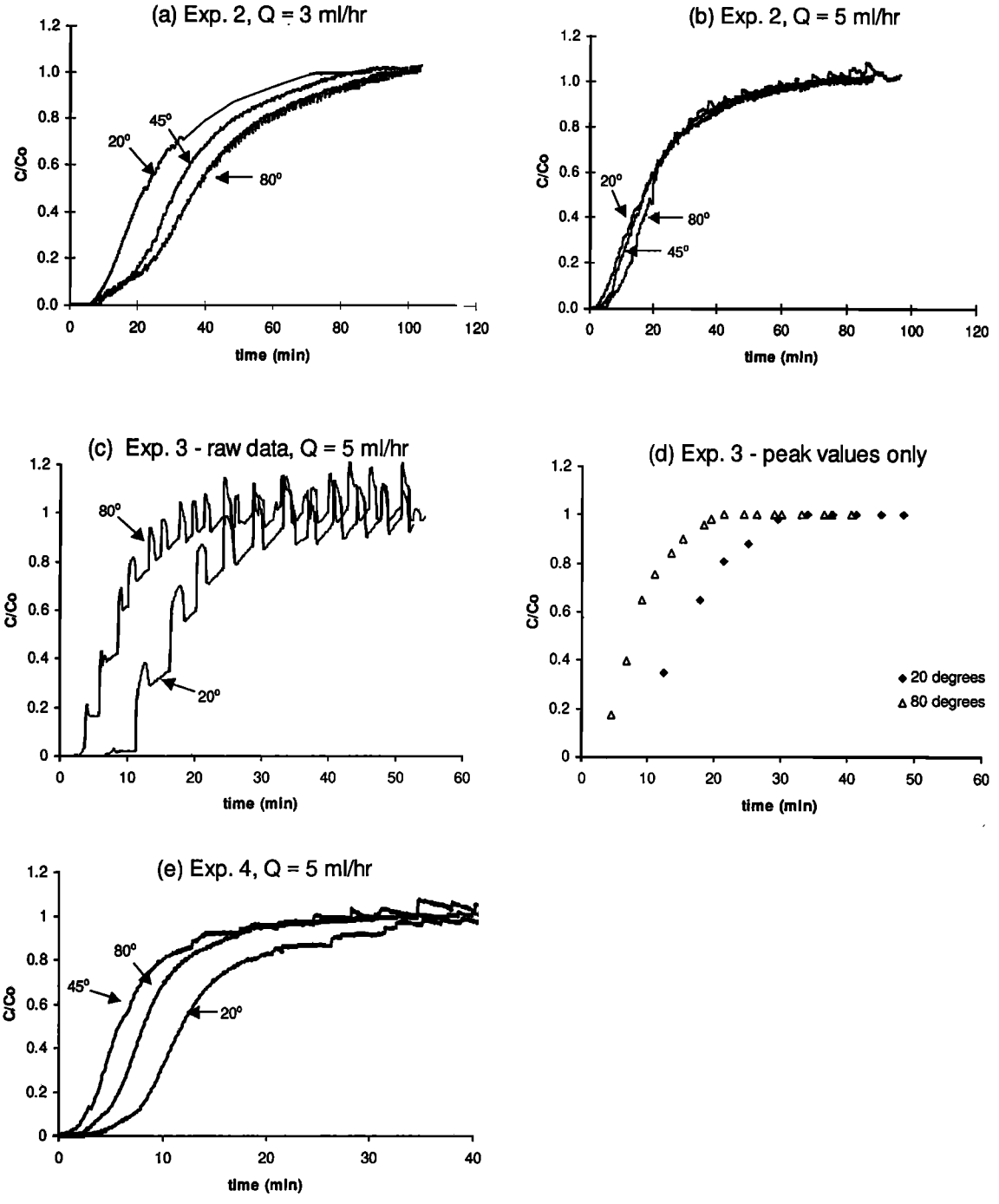

Figure 5. Summary of breakthrough curves from experiments 2–4.

plotted in Figure 6. The peak of the pdf is generally underestimated by all of the models, but the trend at the early and late times is fairly consistent with the data. The calculated values from the axial dispersion and lognormal models give similar fits to the data, except the lognormal model is slightly better at estimating the peak values of the data.

Statistical analysis was performed to compare the measurements with the estimates from the three models. Calculations of the root-mean-square error (RMSE) and the F statistics are summarized in Table 3. The equation for the RMSE is

$$\text{RMSE} = \sqrt{\frac{\sum_{i=1}^{N} (E_{i,\text{calc}} - E_{i,\text{meas}})^2}{N}}, \tag{14}$$

where N is the number of data points, $E_{i,\text{calc}}$ is the calculated value of the pdf, and $E_{i,\text{meas}}$ is the measured value of the pdf. Except for three cases, the reactors-in-series model has the largest RMSE values, while the lognormal model has the smallest values. A smaller RMSE value indicates a better fit;

Table 2. Parameters Obtained From BTCs in Experiments 2–4

Experiment	Q, mL h^{-1}	β, deg	Flow Mode	t_{ave}, min	u_{ave}, cm min^{-1}
2	3	20	snapping rivulet	23.0	1.4
2	3	45	snapping rivulet	31.0	1.0
2	3	80	snapping rivulet	37.0	0.9
2	5	20	snapping rivulet	17.0	1.9
2	5	45	snapping rivulet	17.0	1.9
2	5	80	snapping rivulet	19.5	1.6
3	5	20	pulsating blob	16.5	2.0
3	5	80	pulsating blob	8.5	3.7
4	5	20	steady	12.0	1.7
4	5	45	steady	6.0	3.4
4	5	80	snapping rivulet	8.0	2.5

however, the difference in the RMSE values is not large for the different models.

The F test was also used to compare the performance of the different models and is defined as the ratio between the lack-of-fit mean square (s_r^2) of two models:

$$F = \frac{s^2_{r,\text{model 1}}}{s^2_{r,\text{model 2}}} \tag{15}$$

$$s_r^2 = \frac{\sum_{i=1}^{N} (E_{i,\text{calc}} - E_{i,\text{meas}})^2}{N - K}, \tag{16}$$

where K is the number of independent parameters in each model and $K = 2$ for the three models used in this study. The ratio between the two models must be calculated such that $F \geq 1$. Since three models were used in this study, three F values were calculated for each case to compare the performance of all the models. In order to determine whether one model performs better than another one the calculated F values must be compared to a critical F value (F_{crit}). If the calculated F value is significantly higher than the critical value, model 2 (denominator) describes the measured data better than model 1. Otherwise, the performance of the two models is approximately the same. Only the maximum F value (F_{max}) calculated for each case is summarized in Table 3 since the calculated F values generally did not exceed F_{crit}. The ratios of the models that produced F_{max} are also noted. Of the 27 F values calculated, only five of them exceeded F_{crit} and four of these are F_{max}. The critical F values obtained from an F distribution table [*Chemical Rubber Company*, 1966] are also summarized in Table 3. In order to select F_{crit} the degrees of freedom in the numerator and denominator in F must be known and are equal to $N - 2$ for both. In our results, only F_{max} calculated for experiment 2 at $Q = 5$ mL h^{-1}, 45°, was significantly larger than F_{crit}. These results and the small differences in the RMSE indicate that the three models generally describe the measured travel times nearly equally well.

4.4. Analysis of Breakthrough Curves: Experiment 3

The BTCs from experiment 3 were analyzed by formulating a mechanistic model which accounted for intermittent flow. Under these conditions a series of blobs formed, disconnected, and then coalesced with a pool of water along the bottom (see Figure 4). Solute transport along an intermittent flow path is shown schematically in Figure 7 for a step input concentration change. The blob of water that forms and disconnects near the inlet is assumed to be at the inlet solute concentration (Figure 4a). When the blob coalesces with the residual pool, the volume of water displaced from the pool must have the same volume as the incoming blob if the pool is to remain at equilibrium (Figure 4b). The solute concentration in the blob released from the residual pool is equal to the solute concentration in the pool prior to the blob coalescing with it (Figure 4c). Complete mixing of the solute in the incoming blob with the solute in the pool is assumed to occur before the next blob coalesces with the pool (Figure 4d). The concentration of solute measured at the fracture outlet is zero after one blob is released. After the release of two or more blobs the normalized concentration at the outlet is calculated iteratively as

Table 3. Summary of Calculated Parameters and Performance Statistics for the Transfer Functions[a]

Experiment	Q, mL h^{-1}	β, deg	μ (1), min	σ^2 (2), min^2	Pe (5) and (6)	n (8)	$\mu_{\ln t}$ (10), min	$\sigma^2_{\ln t}$ (11), min^2	RMSE: Axial Dispersion Model, A	RMSE: Reactor Model, R	RMSE: Lognormal Model, L	F Statistics: F_{max}	F_{crit}
2	3	20	28.2	325	3.4	2	23.8	0.34	0.0046	0.0056	0.0044	R/L = 1.64	1.6
2	3	45	35.7	301	5.1	4	32.1	0.21	0.0038	0.0040	0.0037	R/L = 1.16	1.6
2	3	80	39.1	365	5.1	4	35.1	0.21	0.0045	0.0033	0.0039	A/R = 1.88	1.6
2	5	20	20.0	192	3.1	2	16.5	0.40	0.0041	0.0041	0.0059	L/A = 2.06	1.8
2	5	45	21.1	197	3.2	2	17.6	0.37	0.0027	0.0045	0.0034	R/A = 2.80	1.7
2	5	80	23.1	197	3.7	3	19.8	0.31	0.0067	0.0063	0.0051	A/L = 1.71	1.7
4	5	20	14.4	67	4.1	3	10.8	0.37	0.0137	0.0157	0.0126	R/L = 1.55	1.6
4	5	45	7.6	30	2.8	2	6.1	0.42	0.0147	0.0174	0.0116	R/L = 2.17	1.8
4	5	80	9.6	31	3.9	3	8.3	0.29	0.0133	0.0145	0.0117	R/L = 1.55	1.6

[a]Parentheses indicate equation numbers in text.

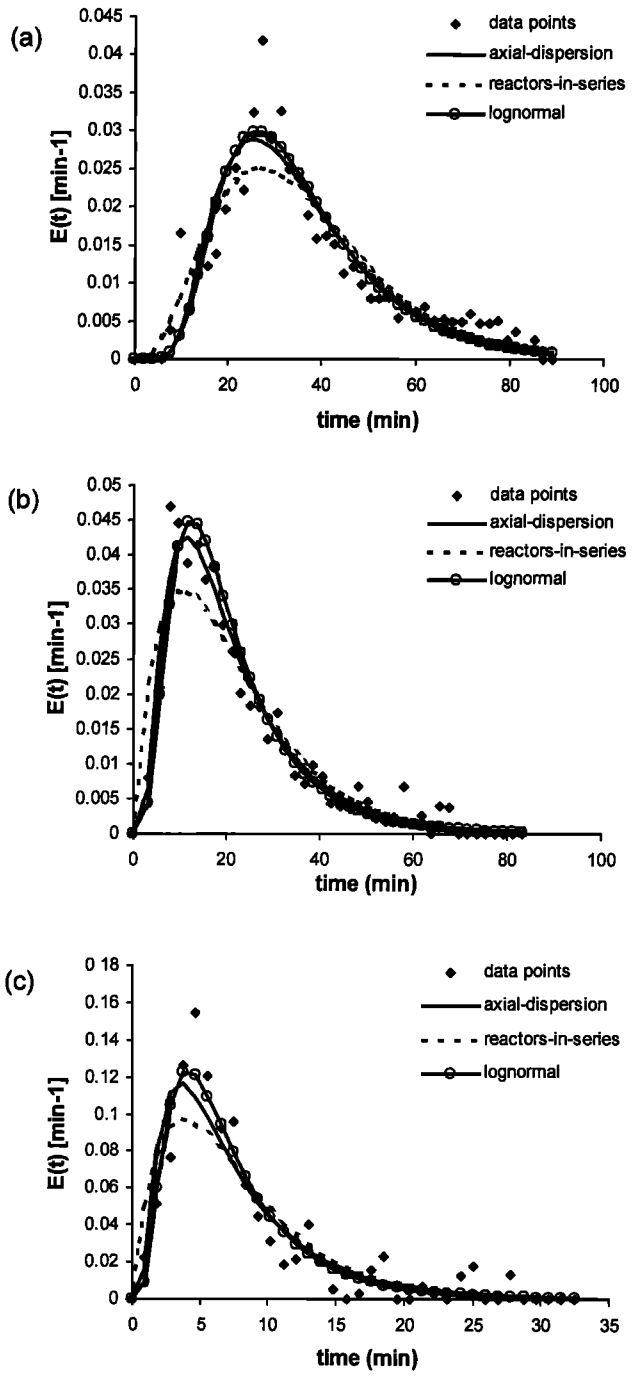

Figure 6. The pdf's of the measured cumulative BTCs at β = 45° and the corresponding estimates with the different transfer function models for (a) experiment 2, Q = 3 mL h^{-1} (b) experiment 2, Q = 5 mL h^{-1} and (c) experiment 4.

$$\left.\frac{C_{\text{out}}}{C_0}\right|_{n_b} = \frac{(M_{\text{blob}} + M_{\text{pool}})|_{n_b-1}}{V_{\text{pool}}C_0} \qquad n_b \geq 2, \tag{17}$$

$$M_{\text{blob}} = V_{\text{blob}}C_{\text{blob}}, \tag{18}$$

$$M_{\text{pool}} = (V_{\text{pool}} - V_{\text{blob}})C_{\text{pool}}, \tag{19}$$

where n_b is the cumulative number of blobs that have formed and disconnected since the introduction of the tracer, M_{blob} is the mass of solute in the incoming blob, M_{pool} is the mass of solute in the residual pool after the incoming blob coalesces with it, V_{blob} is the volume of the blob containing the inlet concentration of solute, V_{pool} is the volume of the residual pool of water, C_{out} is the concentration at the outlet, C_{blob} is the concentration of solute in the blob (assumed equal to C_0 in this model), and C_{pool} is the concentration of solute in the residual pool of water. Substituting (18) and (19) into (17), we obtain

$$\left.\frac{C_{\text{out}}}{C_0}\right|_{n_b} = \frac{V_{\text{blob}}C_{\text{blob}}|_{n_b-1} + (V_{\text{pool}} - V_{\text{blob}})C_{\text{pool}}|_{n_b-1}}{C_0V_{\text{pool}}}$$

$$C_{\text{pool}}|_{n_b-1} = C_{\text{out}}|_{n_b-1} \quad n_b \geq 2. \tag{20}$$

Although (20) is written in terms of the number of blobs, a finite time elapses between two successive blobs reaching the outlet. We assume that the time required for the disconnected blob of water to move through the fracture is minimal compared to the time required for the blob to form and disconnect. This simplification may not be appropriate in longer fractures. The blob velocity is a function of the pressures at the top and bottom of the blob and of the length of the blob [*Nicholl et al.*, 1994; *Su*, 1999].

In Figure 8 the data from experiment 3 are compared with calculations according to (20). The volume of the blob, V_{blob}, used in (20) was obtained by multiplying the flow rate (5 mL h^{-1}) by the average time interval between two successive blobs reaching the outlet, which were 138 s at 80° and 233 s at 20°. These time intervals were obtained by averaging the time between pulses measured in the BTCs. The initial solute concentration in the residual pool is zero, while the normalized concentration in the incoming blob is assumed to be one. The aperture distribution of the fracture replica used in this experiment was not measured; therefore the residual volume of water from experiment 3 could not be calculated from the images. V_{pool} was adjusted to obtain the best fit to the breakthrough curves in Figure 8, resulting in a value of 0.6 mL at 80° and 0.7 mL at 20° for V_{pool}. A smaller residual volume of water is expected at the higher angle since some of the water in the pool drains as the relative influence of gravity increases.

The model assumed only a single capillary pool was present along the flow path, which was consistent with observations of the liquid distribution from experiment 3. The time lag before a concentration was measured in experiment 3 indicates that one blob reached the outlet without solute at 80°, while two blobs reached the outlet without solute at 20°. In order for these results to be consistent with the mechanistic model the number of blobs that reach the outlet without solute should be equal to the number of capillary pools along the flow path. A single capillary pool model is still appropriate for the results at 20° since the initial blob may not have been equal to the inlet solute concentration as we assumed in the model. The tracer was probably introduced when the blob was already of considerable size, resulting in a very small concentration of solute in the first blob ($C_{\text{blob}}/C_0|_{n_t=0} \ll 1$). Therefore, when the next event occurred, the concentration of solute measured at the outlet was still negligible since the solute concentration in the residual pool was minimal.

5. Summary and Conclusions

Laboratory studies were conducted to examine the factors controlling solute transport in unsaturated, inclined fractures. Qualitative aspects of solute transport were identified in a

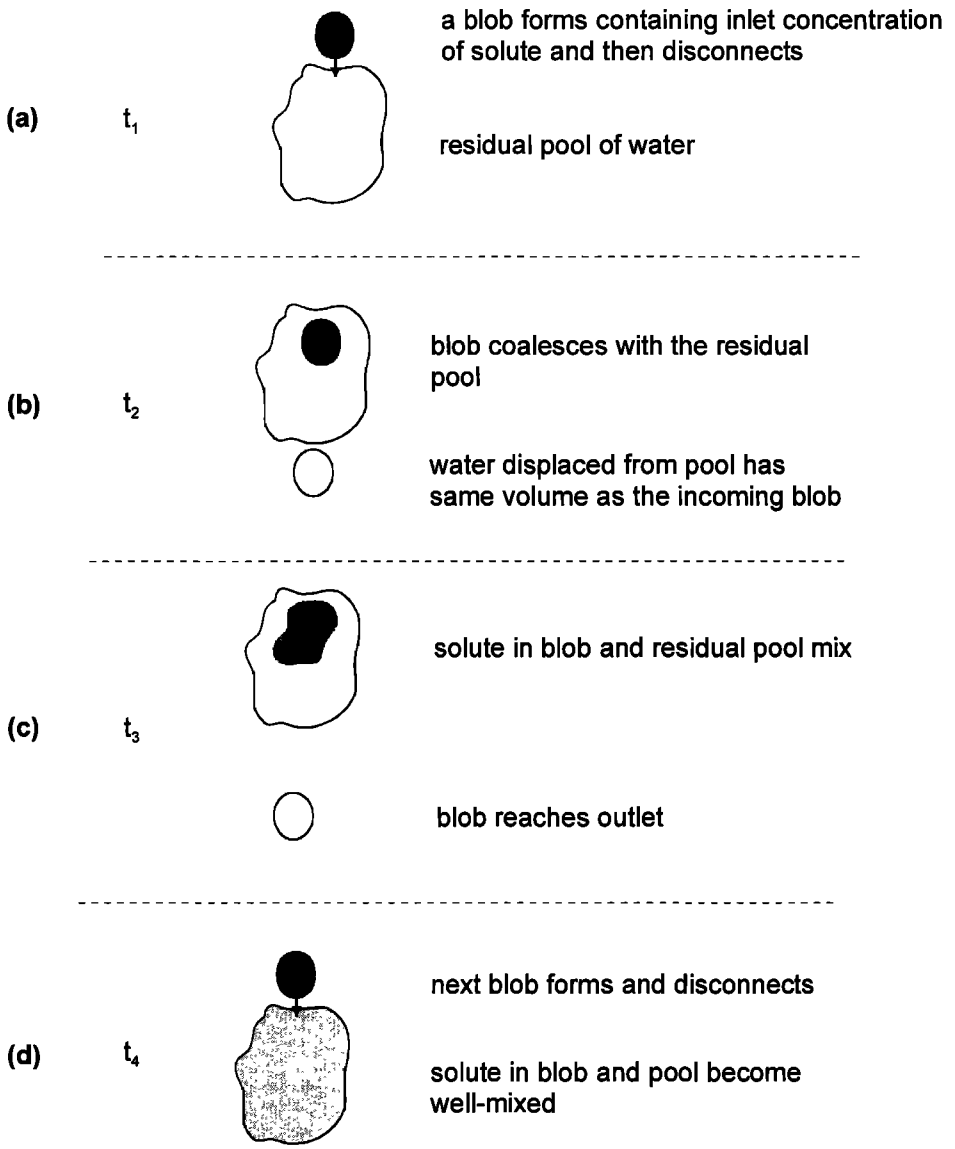

Figure 7. Schematic of solute transport and mixing when flow is undergoing the pulsating blob mode of intermittent flow such as occurred during experiment 3.

miscible dye tracer experiment conducted in a transparent replica of a natural granite fracture. Faster-flowing regions were present within the preferential flow channels. Capillary pools act as long-term sources or sinks for the solute, while transport along rivulets occurred quickly. Additional experiments were conducted to measure the BTCs of a conservative chloride tracer introduced into an established preferential flow path in three different fractures. Intermittent flow had a substantial effect on solute transport in these experiments. Two modes of intermittent flow occurred in two of the experiments: the pulsating blob mode and the snapping rivulet mode. These modes affected the relationship between the travel times of the solute and the relative influence of gravity. During the snapping rivulet mode, the average travel time of the solute actually increased as the relative influence of gravity increased. During the pulsating blob mode, the average travel times of the solute decreased with increasing strength of gravity, as expected. In another experiment where flow changed from steady to intermittent as the

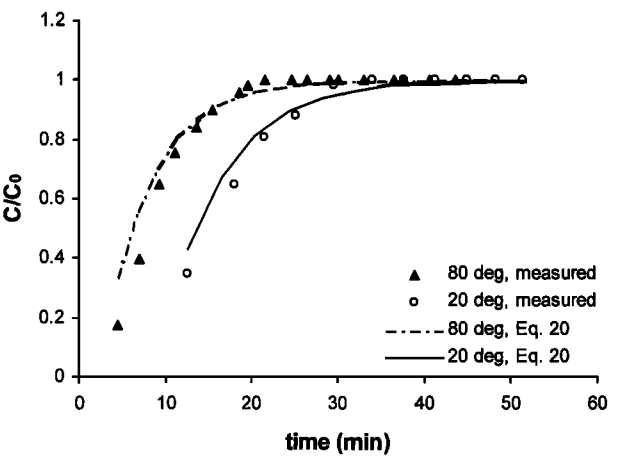

Figure 8. Measured data for experiment 3 and the calculated BTC using (20).

angle of inclination increased, the average travel time increased when flow was intermittent compared to when flow was steady.

The BTCs were analyzed with three transfer function models: the axial dispersion, the reactors-in-series, and the lognormal models. The three models described the measured travel times nearly equally well based on statistical analysis, with the lognormal model generally having the least mean residual error. However, all the models underestimated the peaks of the travel time pdf's. Further studies should be conducted to examine how accurately these models predict solute transport within unsaturated fractures since this study only evaluated the ability of these models to describe the effluent solute travel times. A mechanistic model was also formulated to describe transport when the pulsating blob mode of intermittent flow occurred. The measured BTC was successfully fit to this model, which assumed complete mixing of the blob containing solute with residual pools along the flow path.

These laboratory experiments demonstrate that small-scale mechanisms can substantially impact transport in unsaturated fractures. Other factors affecting transport will inevitably occur at different scales. At larger scales a network of flow channels may join, divide, and enter into perched water bodies. Improving conceptual models for flow and transport in unsaturated fractures requires an understanding of the processes occurring at many different scales.

Acknowledgments. This work was supported by the Director, Office of Energy Research, Office of Health and Environmental Sciences, Biological and Environmental Research Program, of the U.S. Department of Energy under contract DE-AC03-76SF00098. Thanks are owed to Paul Hsieh and David Stonestrom at the USGS, Robert Glass at Sandia National Laboratories, and an anonymous reviewer for their careful reviews of this manuscript. The use of trade names in this publication is provided for information only and does not constitute endorsement or warranty, express or implied, by the USGS or U.S. government as to their suitability, content, usefulness, functioning, completeness, or accuracy.

References

Benjamin, J. R., and C. A. Cornell, *Probability, Statistics, and Decision for Civil Engineers*, 684 pp., McGraw Hill, New York, 1970.

Chemical Rubber Company, *CRC Handbook of Tables for Probability and Statistics*, edited by R. C. Weast, CRC Press, Boca Raton, Fla., 1966.

Chemical Rubber Company, *CRC Handbook of Chemistry and Physics*, edited by D. R. Lide, CRC Press, Boca Raton, Fla., 1994.

Chesnut, D. A., Characterizing the altered zone at Yucca Mountain: The beginning of a testing strategy, paper presented at Third International Conference on High Level Radioactive Waste Management, Am. Nucl. Soc., Las Vegas, Nev., April 12–16, 1992.

Dahan, O., R. Nativ, E. M. Adar, B. Berkowitz, and Z. Ronen, Field observation of flow in a fracture intersecting unsaturated chalk, *Water Resour. Res.*, *35*(11), 3315–3326, 1999.

Doughty, C., Investigation of conceptual and numerical approaches for evaluating moisture, gas, chemical and heat transport in fractured unsaturated rock, *J. Contam. Hydrol.*, *38*, 69–106, 1999.

Dunnivant, F. M., et al., Water and radioactive tracer flow in a heterogeneous field-scale system, *Ground Water*, *36*(6), 949–958, 1998.

Fabryka-Martin, J. T., A. V. Wolfsberg, A. V. Dixon, P. R. Dixon, S. Levy, J. Musgrave, and H. J. Turin, Summary report of chlorine-36 studies: Sampling, analysis and simulation of chlorine-36 in the Exploratory Studies Facility, *Los Alamos Natl. Lab. Rep. LA-CST-TIP-96-002*, Los Alamos Natl. Lab., Los Alamos, N. M., 1996.

Geller, J. T., G. Su, and K. Pruess, Preliminary studies of water seepage through rough-walled fractures, *LBNL Rep. 38810*, Lawrence Berkeley Natl. Lab., Berkeley, Calif., 1996.

Geller, J. T., H. Y. Holman, G. Su, K. Pruess, and J. C. Hunter-Cevera, Flow dynamics and potential for biodegradation of organic contaminants in fractured rock vadose zone, *J. Contam. Hydrol.*, *43*, 63–90, 2000.

Glass, R. J., Modeling gravity driven fingering in rough-walled fractures using modified percolation theory, paper presented at Fourth International Conference on High Level Radioactive Waste Management, Am. Nucl. Soc., Las Vegas, Nev., April 26–30, 1993.

Glass, R. J., and M. J. Nicholl, Physics of gravity fingering of immiscible fluids within porous media: An overview of current understanding and selected complicating factors, *Geoderma*, *70*, 133–163, 1996.

Glass, R. J., G. H. Oosting, and T. S. Steenhuis, Preferential solute transport in layered homogeneous sands as a consequence of wetting front instability, *J. Hydrol.*, *110*, 87–105, 1989.

Jury, W. A., Simulation of solute transport using a transfer function model, *Water Resour. Res.*, *18*(2), 363–368, 1982.

Jury, W. A., and K. Roth, *Transfer Functions and Solute Movement Through Soil: Theory and Application*, 239 pp., Birkhäuser Boston, Cambridge, Mass., 1990.

Jury, W. A., J. S. Dyson, and G. L. Butters, Transfer function model of field-scale solute transport under transient water flow, *Soil Sci. Soc. Am. J.*, *54*, 327–332, 1990.

Levenspiel, O., Nonideal flow, in *Chemical Reaction Engineering*, 2nd Ed., pp. 254–325, John Wiley, New York, 1972.

Liu, B., J. Fabryka-Martin, A. Wolfsberg, B. Robinson, and P. Sharma, Significance in apparent discrepancies in water ages derived from atmospheric radionuclides at Yucca Mountain, Nevada, *Los Alamos Natl. Lab. Rep. LA-UR-95-572*, Los Alamos Natl. Lab., Los Alamos, N. M., 1995.

Nativ, R., E. Adar, O. Dahan and M. Geyh, Water recharge and solute transport through the vadose zone of fractured chalk under desert conditions, *Water Resour. Res.*, *31*(2), 253–261, 1995.

Nicholl, M. J., R. J. Glass, and S. W. Wheatcraft, Gravity-driven infiltration instability in initially dry nonhorizontal fractures, *Water Resour. Res.*, *30*(9), 2533–2546, 1994.

Nitao, J., and T. Buscheck, Infiltration of a liquid front in an unsaturated, fractured porous medium, *Water Resour. Res.*, *27*(8), 2099–2112, 1991.

Persoff, P., and K. Pruess, Two-phase flow visualization and relative permeability measurement in natural rough-walled rock fractures, *Water Resour. Res.*, *31*(5), 1175–1186, 1995.

Pruess, K., On water seepage and fast preferential flow in heterogeneous, unsaturated rock fractures, *J. Contam. Hydrol.*, *30*, 333–362, 1998.

Pruess, K., B. Faybishenko, and G. S. Bodvarsson, Alternative concepts and approaches for modeling flow and transport in thick unsaturated zones of fractured rocks, *J. Contam. Hydrol.*, *38*, 281–322, 1999.

Su, G. W., Flow dynamics and solute transport in unsaturated rock fractures, *Rep. LBNL-44440*, Lawrence Berkeley Natl. Lab., Berkeley, Calif., Oct., 1999.

Su, G. W., J. T. Geller, K. Pruess, and F. Wen, Experimental studies of water seepage and intermittent flow in unsaturated, rough-walled fractures, *Water Resour. Res.*, *35*(4), 1019–1037, 1999.

Tokunaga, T., and J. Wan, Water film flow along fracture surfaces of porous rock, *Water Resour. Res.*, *33*(6), 1287–1295, 1997.

Wang, J. S. Y., and T. N. Narasimhan, Hydrologic mechanisms governing fluid flow in a partially saturated, fractured, porous medium, *Water Resour. Res.*, *21*(12), 1861–1874, 1985.

Zhang, R., Prediction of solute transport using a transfer function model and the convection-dispersion equation, *Soil Sci.*, *160*(1), 18–27, 1995.

J. T. Geller and K. Pruess, Earth Sciences Division, Lawrence Berkeley National Laboratory, 1 Cyclotron Road, Building 50E, Berkeley, CA 94720, USA. (jtgeller@lbl.gov; k_pruess@lbl.gov)

J. R. Hunt, Department of Civil and Environmental Engineering, University of California at Berkeley, 631 Davis, MC 1710, Berkeley, CA 94720-1710, USA. (hunt@ce.berkeley.edu)

G. W. Su, Water Resources Division, U.S. Geological Survey, 345 Middlefield Road, MS 421, Menlo Park, CA 94025, USA. (gracesu@usgs.gov)

(Received November 13, 2000; revised April 20, 2001; accepted May 23, 2001.)